International Journal of Nanomedicine

Dovepress
Taylor & Francis Group

Open Access Full Text Article

ORIGINAL RESEARCH

# Bladder Defect Repair by Polycaprolactone/ Gelatin Nanofiber Scaffolds Loaded with Mitomycin Through Anti-Fibrotic Effects

Congcong Yang[1,*], Jianyou Xia[2,*], Lunjie Zhao[3,*], Jianping Tao[1,*], Dan Li[1], Renxi Zhu[1], Qiang Wang[1], Haichen Shen[1], Baochao Zhang[4], Yujie Xu[1]

[1]Department of Urology, The First Affiliated Hospital of Wannan Medical College, Wuhu, 241001, People's Republic of China; [2]Department of Urinary Surgery, General Hospital of Central Theater Command, Wuhan, 430012, People's Republic of China; [3]Department of Urology, Chinese People's Armed Police Forces Anhui Provincial Corps Hospital, Hefei, 230001, People's Republic of China; [4]Department of Urology, Nanjing First Hospital, Nanjing Medical University, Nanjing, 210000, People's Republic of China

*These authors contributed equally to this work

Correspondence: Yujie Xu, Department of Urology, The First Affiliated Hospital of Wannan Medical College, Wuhu, 241001, People's Republic of China, Email xyj_1213@126.com; Baochao Zhang, Department of Urology, Nanjing First Hospital, Nanjing Medical University, Nanjing, 210000, People's Republic of China, Email zhang_bch@126.com



**Background:** In recent years, bladder defect repair has emerged as a critical issue in urological tissue engineering. Traditional treatment methods, such as autologous tissue transplantation and synthetic material repair, are limited by factors such as scarce donor sources, immune rejection, and postoperative fibrosis. Consequently, the development of nanofiber materials with bionic structures, biocompatibility, and anti-fibrotic capabilities has become a research hotspot. This research addressed the clinical needs associated with tuberculous bladder contracture, chronic cystitis, traumatic bladder rupture, and malignant tumors requiring partial cystectomy (such as localized non-muscle-invasive bladder cancer and urachal cancer), among other conditions. Excessive fibrotic scar formation following bladder surgery or injury is a primary contributor to reduced bladder compliance, diminished capacity, and impaired contractile function.

**Methods:** Using electrospinning technology, we designed and prepared composite nanofibers with varying proportions (9:1, 7:3, 5:5) of polycaprolactone (PCL) and gelatin (GEL). By conducting various experiments such as scanning electron microscopy (SEM), water contact angle (WCA) analysis, mechanical performance evaluation, and Fourier transform infrared spectroscopy (FTIR), the PCL/GEL (7:3) composite material was ultimately selected as the one with the best overall performance.

**Results:** Its fiber diameter was 612.14 ± 105.46 nm, water contact angle was 107.23°, and mechanical properties (tensile strength: 3.84 ± 0.5 MPa, elongation at break: 118.42 ± 4%, Young's modulus: 19.50 ± 4.6 MPa). To enhance its anti-fibrotic properties, we incorporated mitomycin C (MMC) into the nanofiber matrix and prepared PCL/GEL/MMC nanofiber materials through blending and spinning. We then established a partial cystectomy model in rats, implanted the PCL/GEL/MMC nanofiber materials, and performed bladder imaging four weeks post-surgery to assess bladder capacity and morphological recovery. The CCK-8 assay was performed on days 1, 3, and 7, demonstrating that smooth muscle cells (SMCs) and endothelial cells (ECs) can effectively adhere, survive, and proliferate on these fibrous membranes, thereby confirming their biocompatibility. The anti-fibrotic properties of the materials were evaluated using immunofluorescence staining (IF)and immunohistochemical analysis (IHC).

**Conclusion:** The experimental results demonstrated that PCL/GEL nanofiber materials loaded with 0.02% MMC exhibited excellent biocompatibility and anti-fibrotic effects in bladder defect repair, providing a theoretical basis for their potential clinical application.

**Keywords:** bladder defect, electrospinning, mitomycin, anti-fibrotic therapy

## Introduction

Bladder diseases such as tuberculosis and chronic cystitis can lead to decreased bladder capacity. Muscle-invasive bladder cancer often requires partial or radical cystectomy, a major surgery that damage the bladder's function of storing

https://doi.org/10.2147/IJN.S574989
Received: 5 November 2025
Accepted: 2 February 2026
Published: 11 February 2026

and emptying urine. Bladder injuries can also result in significant tissue loss. All the above-mentioned diseases require bladder enlargement or bladder repair.[1,2] Currently, the primary treatment often involves the use of ileal to augment the bladder.[3] Although this technique can restore bladder function, it is associated with significant trauma, postoperative urinary tract infections, intestinal complications, and metabolic complications.[4] Consequently, there is an urgent clinical need for innovative artificial bladder substitutes.

The complex biochemical process of bladder tissue regeneration requires two key cellular players: epithelial cells (ECs), which mediate epithelialization, and smooth muscle cells (SMCs), which facilitate the formation of smooth muscle bundles.[5] Bladder fibrosis is a prevalent issue encountered in bladder tissue engineering.[6] Therefore, the development of a bladder defect repair material that demonstrates anti-fibrotic properties is of considerable significance. Electrospinning technology is capable of producing nanofiber membranes or scaffolds with controllable thickness, diverse morphologies, and varying porosities.[7] This method is widely applied in tissue engineering for regenerating various tissues, including skin, blood vessels, nerves, bone, cartilage and other tissue types.[8–12] Electrospinning technology demonstrates significant potential in the reconstruction of urinary tract tissues. The high degree of similarity between electrospun membranes and natural extracellular matrix (ECM) facilitates enhanced cell adhesion and proliferation.[7,13] Bladder repair materials currently employed in clinical practice and research primarily fall into two categories: natural biomaterials and synthetic polymers. Natural biomaterials mainly include acellular bladder matrix (BAMG) and small intestinal submucosa (SIS), whereas synthetic polymers encompass a broader range of materials, such as polylactic acid (PLA), polyglycolic acid (PGA), and their copolymers (PLGA).[14]

Mitomycin C (MMC) is a chemotherapy agent derived from streptomyces caesius, known for its ability to inhibit the replication of tumor cell DNA. This mechanism underlies its anti-tumor and antibiotic properties.[15] MMC possesses the capability to inhibit mitosis, fibroblast proliferation, protein and collagen synthesis. By modulating fibroblast proliferation through the TGF-β/Smad signaling pathway, MMC plays a pivotal role in tissue repair and the reduction of scar formation.[16] Among numerous synthetic biopolymers, PCL has been widely used in the construction of tissue engineering scaffolds due to its excellent biocompatibility, controllable slow degradation property (usually over 2 years), and superior mechanical flexibility and processability. Particularly, it is suitable for processes such as electrospinning, facilitating the fabrication of nanofibers that mimic the topological structure of natural extracellular matrix.[17] However, its inherent hydrophobicity and absence of bioactive binding sites restrict initial cell adhesion and proliferation. In contrast, GEL, a hydrolyzed derivative of collagen, is abundant in arginine-glycine-aspartic acid (RGD) motifs, which confer high cell affinity, facilitate cell migration and differentiation, and enable enzyme-responsive degradation.[18] Nevertheless, its limited mechanical integrity and rapid dissolution in aqueous environments hinder its use as a standalone load-bearing scaffold. Combining PCL and GEL represents a well-established strategy to exploit their complementary properties: PCL serves as a structural backbone providing mechanical stability, while GEL imparts a bioactive interface on the fiber surface or within the matrix.[19] Prior studies have shown that PCL-GEL composite nanofibers enhance epithelialization in skin tissue regeneration and support Schwann cell migration in neural guidance conduits.[20,21] These successful applications provide strong rationale and a solid foundation for extending this material system to bladder repair.

Previous investigations into the use of electrospun membranes for bladder repair have predominantly emphasized structural regeneration, with limited attention to strategies addressing postoperative complications, particularly fibrosis. This study forms a meaningful contrast and complement to the previously published work by our research group using PLLA/GEL microfibers. Both studies jointly confirm the synergistic potential of MMC and gelatin-based composite scaffolds in bladder repair. This study focuses on the design, optimization, and comprehensive in vitro investigation of the anti-fibrotic mechanism of the PCL/GEL platform. Notably, this work is the first systematic report on PCL/GEL nanofibers loaded with MMC for bladder tissue repair, demonstrating significant and irreplaceable novelty.[22] In this experiment, we prepared PCL/GEL nanofiber scaffolds loaded with MMC using electrospinning. The scaffold exhibited optimal mechanical properties, hydrophilicity, and biocompatibility in a series of tests. Furthermore, in a rat bladder defect model, it effectively promoted the regeneration of SMCs and ECs, stimulated angiogenesis, and inhibited fibrosis. Our results propose an advanced strategy that not only opens new avenues for bladder reconstruction but also elucidates

key mechanisms in bladder tissue regeneration. The preparation of PCL/GEL/MMC nanofiber membrane and its application in bladder defect repair are illustrated in Figure 1.

# Materials and Methods

## Materials

PCL (Mw = 50 kDa), Type A gelatin, MMC (purity ≥ 98%), and hexafluoroisopropanol (HFIP) were acquired from Aladdin Chemistry Co., Ltd. (China). Trypsin-EDTA Solution (BL512A) and Cell Counting Kit-8 (CCK8, BS350B) were provided by Biosharp. Dulbecco's Modified Eagle Medium (DMEM, catalog no. U21-265B) was obtained from YOBIBIO, and fetal bovine serum (FBS, catalog no. 10270–106) was purchased from Gibco. Human bladder epithelial cells (ECs, SNP-H012) and human ureter smooth muscle cells (SMCs, SNP-H270) were sourced from Sunncell Biotechnology. The primary antibodies used in this research included anti-Smad2 (ab63576), anti-alpha Smooth Muscle Actin (α-SMA, ab7817), anti-pan Cytokeratin (AE1/AE3, ab80826), and anti-CD31 (ab28364), all supplied by Abcam.

## Preparation of PCL/GEL Nanofiber

Dissolved PCL/GEL (9:1/7:3/5:5) in HFIP to prepare a 15% concentration electrospinning solution. Once the solution was completely mixed to ensure uniformity, it was loaded into a 10 mL syringe and mounted on the electrospinning apparatus. To conduct the experiment, a 23G stainless steel blunt needle tip is required, with a fixed distance of 15 cm between the needle tip and the collection device. The solution should be delivered at a constant rate of 1.5 mL/h. Furthermore, the relative humidity of the experimental environment must be maintained at 50%, and the applied voltage should be set to 18 kV. Following fabrication, the PCL/GEL (9:1, 7:3, 5:5) nanofibrous membranes were left to dry under ambient conditions overnight. The optimal proportion of the PCL/GEL nanofiber membrane exhibiting superior physicochemical properties was then determined through a systematic screening process. Next, either 0.02% or 0.1% MMC was incorporated into the prepared 15% PCL/GEL solution, which was then reintroduced into the electrospinning machine. The previously described procedure was repeated to fabricate PCL/GEL/MMC nanofiber membranes.

## Morphological Analysis of Nanofiber Membrane

The morphology of the nanofiber membrane was examined via scanning electron microscopy (SEM, TESCAN MIRA LMS, Czech Republic) operated at an accelerating voltage of 8 kV. To improve surface conductivity, the samples were

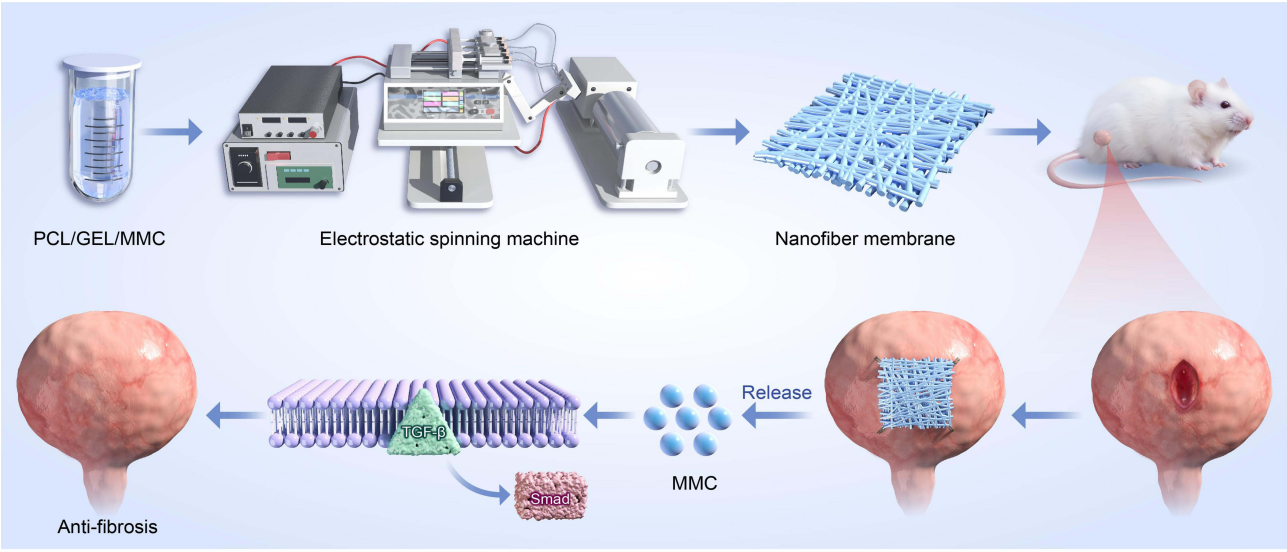


**Figure 1** Preparation process of PCL/GEL/MMC nanofiber membrane and experimental procedure for bladder repair in rats.


https://doi.org/10.2147/IJN.S574989

coated with a fine layer of gold (Au) using a sputter coater before imaging. The mean fiber diameters were measured from the obtained SEM micrographs employing ImageJ software.

## Fourier Transform Infrared Spectroscopyx

The primary changes in the chemical composition of the polymer blend were confirmed by Fourier Transform Infrared Spectroscopy (FTIR) using a Thermo Fisher Scientific Nicolet iS20 spectrometer (USA). The test was conducted in attenuated total reflection mode. The specific parameters were as follows: the spectral scanning range was from 4000 to 400 $cm^{-1}$, the resolution was 4 $cm^{-1}$, and the cumulative scanning times were 32. All spectra were automatically baseline corrected.

## Investigation of Mechanical Properties

The mechanical performance of nanofiber membranes, each with dimensions of 4 cm × 1 cm, were evaluated with a universal electronic testing machine (INSTRON 3367, USA). The system utilized a 100 N load cell and was configured with a 1 cm gap between the clamps. The samples were subjected to testing at a constant crosshead speed of 2 mm/min until failure occurred, and tensile strength, elongation at break, and Young's modulus were derived from the resulting data (n = 3).

## Water Contact Angle

The wettability of each nanofiber membrane was evaluated by determining the static contact angle using a precision measurement device (SDC-350KS, Dongguan Sheng Ding, China). In this process, a 0.25 μL droplet of deionized water was carefully placed on the membrane surface, and a photograph was taken after 2 seconds. The contact angle was calculated by determining the angle formed between the droplet's tangent line and the solid-liquid boundary, providing an accurate evaluation of the surface's wetting behavior. Five different positions were randomly selected for measurement on each sample, and the results were expressed as "mean ± standard deviation". All the contact angle data reported in the text were independently measured five times (n = 5).

## Drug Release Study

The in vitro release profile of MMC was analyzed using high-performance liquid chromatography (HPLC). Briefly, a PCL/GEL/MMC sample (2 × 2 cm) was placed into a centrifuge tube containing 20 mL of phosphate-buffered saline (PBS). The tube was placed in a temperature-regulated shaker and incubated at 37°C under continuous agitation at 100 rpm. At specified time points, 1 mL of the release medium was sampled for analysis, and the same volume of fresh pre-warmed PBS was promptly added to ensure a constant volume and stable physiological environment.

## Biocompatibility Assay

Circular PCL/GEL and PCL/GEL/MMC membrane discs, each with a 25 mm diameter, were fabricated and mounted onto culture inserts. Prior to cell seeding, the membranes were sterilized using ultraviolet irradiation, followed by treatment with 75% ethanol for 30 minutes, and then transferred into a 24-well plate. ECs and SMCs were suspended in DMEM medium supplemented with 10% FBS and seeded onto the membrane surfaces at a density of $3.0 \times 10^4$ cells/mL. After incubation at 37°C in a humidified 5% $CO_2$atmosphere for 1, 4, and 7 days, the samples were collected, fixed, and analyzed on their bottom side via SEM.

Cells cultured on the membranes were rinsed three times with PBS and fixed with 4% paraformaldehyde for 30 min at room temperature. The samples were then incubated with primary antibodies overnight at 4°C. After three additional washes with PBS, the cells were exposed to secondary antibodies for 45 min at room temperature. Following a 24-hour incubation on the fixed membranes, cell morphology and adhesion were assessed by fluorescently labeling α-SMA, AE1/AE3, and nuclear DNA.

The circular membrane was sterilized according to the previously outlined procedure. ECs and SMCs were then seeded onto the sterilized membrane at a density of $2.0 \times 10^4$ cells/mL. Following incubation for 1, 3, and 7 days, the CCK-8 reagent was introduced into the culture medium and allowed to incubate with the cells for an additional 2 hours.

Subsequently, 200 μL of the supernatant was transferred to a 96-well plate, and absorbance was read at 450 nm using a microplate spectrophotometer to evaluate cell viability.

## Animal Experiment

The animal experiments were carried out in compliance with the National Guidelines for the Care and Use of Laboratory Animals in China. All protocols were reviewed and approved by the Institutional Animal Care and Use Committee of Wannan Medical College (Approval Number: LLSC-2022-137). The rats were kept under controlled conditions with a 12-hour light/dark cycle, maintained at a stable temperature of 25°C, and supplied with standard chow and water available freely throughout the study.

Forty healthy female rats, each weighing around 200 grams, were randomly assigned to four experimental groups (n = 10 per group): tissue-engineered PCL/GEL, PCL/GEL/0.02% MMC, PCL/GEL/0.1% MMC, and a blank control group. No surgical intervention was conducted in the blank control group. For the remaining three groups, a full-thickness 5 mm × 5 mm defect was surgically induced by excising a portion of the anterior bladder wall. Rats were anesthetized with an intraperitoneal injection of a mixture of ketamine (90 mg/kg, Pfizer) and xylazine (10 mg/kg, Pfizer). The depth of anesthesia was assessed by the absence of a pedal withdrawal reflex. The entire surgical process was performed in a sterile environment, and a heating pad was used to maintain the body temperature of the rats at 37°C. We initially attempted to establish a "blank defect control group", in which full-thickness bladder defects were created and only the muscular layer and skin were sutured, without implantation of any repair materials. However, all animals in this group (n = 4) either died or were humanely euthanized within 24–48 hours postoperatively due to severe urinary peritonitis, intra-abdominal infection, and systemic deterioration. These findings demonstrate that a 5 mm × 5 mm full-thickness bladder defect in the rat model does not resolve through spontaneous contraction or natural healing, and effective surgical intervention is required to restore structural integrity and prevent life-threatening complications. Consequently, subsequent experiments were designed to compare the relative efficacy of various repair materials under conditions where intervention is essential.

Following defect creation, the bladder injuries were repaired by implanting PCL/GEL, PCL/GEL/0.02% MMC, or PCL/GEL/0.1% MMC nanofibrous membranes, respectively. Using 5–0 absorbable sutures, appropriately sized PCL/GEL and PCL/GEL/0.02% MMC nanofiber membranes were implanted into the defect site utilizing intermittent suturing techniques. Postoperatively, each rat was housed individually in its own cage and allowed unrestricted access to food and water throughout the recovery period.

## Retrograde Cystography

Twelve weeks post-surgery, retrograde cystography was carried out. After inducing general anesthesia, the rats were positioned obliquely on the imaging table Given the narrow diameter of the rat urethra, an epidural catheter was utilized as a urinary catheter and gently advanced into the urethra until urine discharge was confirmed. Subsequently, iohexol was administered through the catheter using a 1 mL syringe and monitored in real time with a digital X-ray fluoroscopy system to evaluate bladder morphology and function.

## Histological and Immunohistochemical Analyses

Following the completion of retrograde cystography, the experimental rats were humanely euthanized through cervical dislocation in accordance with established animal welfare protocols. The anterior bladder wall specimens were collected and immersed in 10% paraformaldehyde for 48 hours to ensure complete fixation. After fixation, the tissue samples were rinsed, dehydrated using a graded ethanol series, embedded in paraffin wax, and sectioned into 5 μm slices. These sections were then subjected to hematoxylin and eosin (HE) staining for histological examination. To evaluate collagen accumulation, Masson's trichrome and Sirius red staining were performed, with images acquired at 100× magnification; representative fields were selected for detailed analysis.

Immunohistochemical (IHC) staining was employed to evaluate the expression of TGF-β, Smad2, and CD31 in bladder tissues.

## Statistical Analysis

The data are expressed as mean ± standard deviation (Mean ± SD). One-way ANOVA was conducted for statistical evaluation using GraphPad Prism software, and differences were considered statistically significant at a $P$-value < 0.05.

# Results and Discussion

## Morphology and Structure of Fibers

Nanofiber scaffolds produce through electrospinning technology can establish a specialized environment that promotes the systematic growth of cells and tissues.[23] These scaffolds possess the capability to construct an artificial ECM that encompasses intricate fibrous structures, including collagen, glycosaminoglycans, elastin, and other components.[24] Due to their distinctive architecture, these scaffolds provide biochemical and mechanical support to adjacent cells.[25,26] A suitable fiber diameter is conducive to the formation of a three-dimensional interconnected network with appropriate pore size and high porosity. It not only provides a huge specific surface area for cell migration and spreading, but also ensures the adequate penetration of oxygen and nutrients as well as the efficient removal of metabolic wastes, which is the key to cell compatibility.[27]

Scanning electron microscopy (SEM) images (Figure 2A–C) show that the nanostructures of PCL/GEL nanofiber mats with ratios of 9:1, 7:3, and 5:5 are randomly but uniformly distributed. These mats exhibited smooth fiber surfaces, characterized by a substantial surface area and a distinct porous structure. Notably, neither bead nor spindle-on-a-string phenomena were observed. The diameter distribution and mean fiber sizes were evaluated using ImageJ software. The analysis revealed that the PCL/GEL nanofibers exhibited diameters within the following range, specifically those with ratios of 9:1, 7:3, and 5:5, were measured at 483.14 ± 76.93 nm, 612.14 ± 105.46 nm, and 1262.56 ± 185.37 nm (Figure 2D–F), respectively. In the PCL/Gelatin composite system, as the relative content of gelatin increases (ie, the proportion of PCL decreases accordingly), the average diameter of the prepared nanofibers shows an increasing trend. This is mainly attributed to the different rheological properties (such as viscosity and conductivity) of the gelatin solution and the PCL solution.[28]

The electrospun PCL/GEL membranes with a 7:3 ratio exhibit fiber diameters ranging from 612 nm, a dimension widely recognized as the "ideal topological range" for eliciting favorable cellular responses.[29] This scale effectively

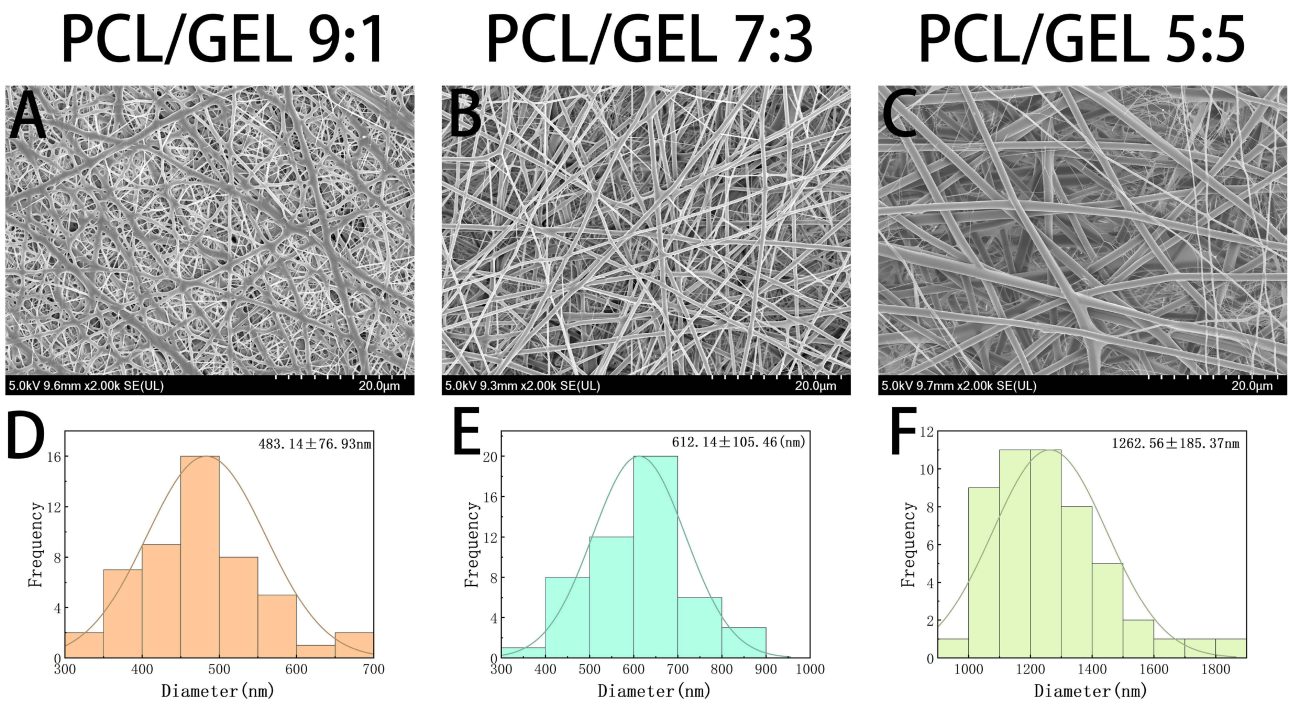


**Figure 2** SEM images (**A**–**C**) of PCL/GEL at ratios of 9:1, 7:3, and 5:5, and their corresponding diameter distributions (**D**–**F**).


https://doi.org/10.2147/IJN.S574989

mimics the physical architecture of collagen fibers in the natural extracellular matrix (ECM), thereby providing a highly biomimetic microenvironment that supports the growth of bladder epithelial cells and smooth muscle cells and enhances their initial adhesion and recognition.[30] This is also one of the reasons why we chose the 7:3 ratio of PCL/GEL electrospun membranes to load MMC for subsequent steps.

## Measurement of Water Contact Angle

The surface wettability-whether hydrophobic or hydrophilic - significantly affects cellular activities, especially cell adhesion and proliferation. Hydrophilic surfaces typically enhance cell-material interactions, thereby exerting a substantial influence on cellular performance.[31] PCL is inherently hydrophobic due to the presence of non-polar functional groups in its structure,[32] which limits its ability to absorb water. Conversely, GEL contains polar functional groups such as amino and carboxyl moieties that readily form hydrogen bonds with water, contributing to higher hydrophilicity and improved moisture retention.[33] The water contact angles of PCL/GEL nanofiber materials with ratios of 9:1, 7:3, and 5:5 are shown in photographic documentation as illustrated in Figures 3A–C. Consequently, the experimental results demonstrate that as the gelatin content increases, the water contact angle of the nanofibrous scaffold gradually decreases, reflecting enhanced surface hydrophilicity (Figures 3D).

## Mechanical Characterization

Bladder tissue engineering aims to develop materials that promote tissue regeneration and sustain the mechanical functionality of the bladder until complete restoration is achieved. Both processes are significantly influenced by the mechanical properties of the material.[34] The physical stimuli provided by biomaterials play a crucial role in influencing the proper morphogenesis, maintenance, and repair of tissues. Furthermore, the biomechanical characteristics of these materials must enable a consistent cycle of contraction and expansion while effectively preventing urine leakage and

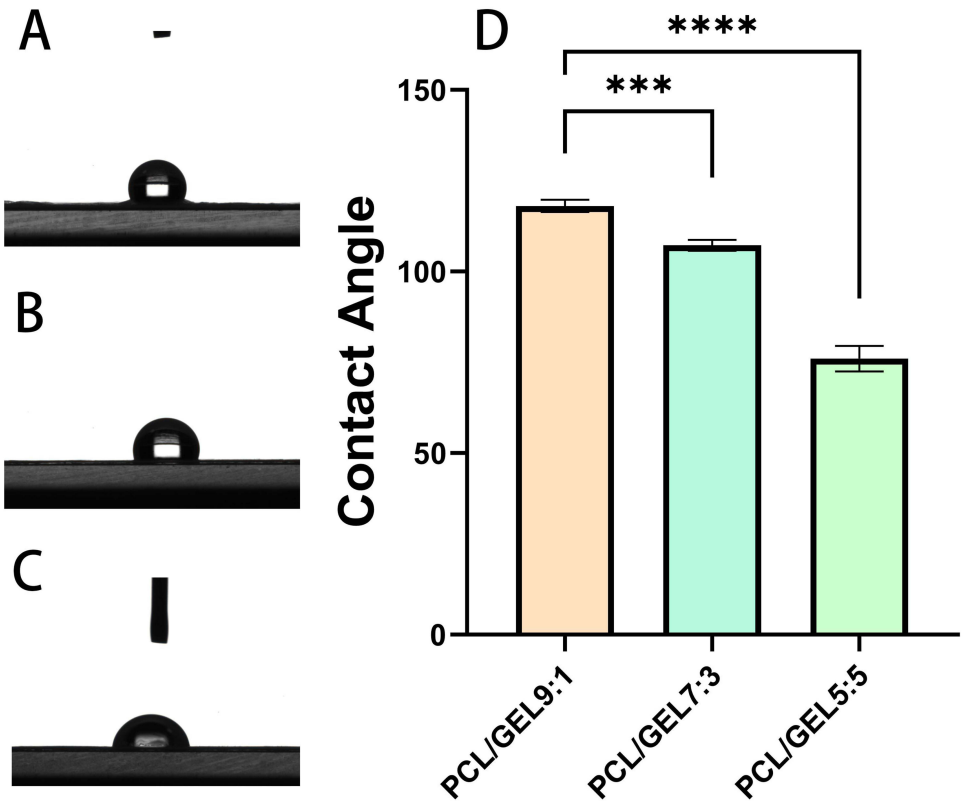


**Figure 3** Photographic records (**A**–**C**) and results (**D**) of water contact angle assessment of PCL/GEL nanofiber membranes with ratios of 9:1, 7:3, and 5:5. (***$P$-value < 0.001, ****$P$-value < 0.0001).


https://doi.org/10.2147/IJN.S574989

stent deformation.[35] Therefore, the mechanical properties are essential in determining the optimal ratio of PCL/GEL nanofibers for effective bladder repair.

Figure 4A displays the evaluated mechanical properties. The tensile strain was determined at the peak of the stress–strain curve, and Young's modulus was calculated from the slope of the linear region of the curve. Of all the samples tested, PCL/GEL (9:1) showed the greatest tensile strain and elongation at break, whereas PCL/GEL (5:5) exhibited the lowest values (Figures 4B and C). The magnitude of Young's modulus served as an indicator of a material's rigidity. Among the three scaffold types examined, PCL/GEL (7:3) exhibited the highest Young's modulus, achieving a value of 20.10 ± 2.18 MPa (Figure 4D).

As a synthetic polymer, PCL exhibits excellent mechanical strength, structural stability, and tunable degradability. In contrast, GEL, as a natural polymer, provides inherent biocompatibility, specific cell recognition sites (such as RGD sequences), and enhanced hydrophilicity. Composite nanofibers fabricated via blend electrospinning integrate the advantages of both components, resulting in overall performance that surpasses that of individual PCL or GEL scaffolds.[18] In addition, the mechanical property data of the materials in this study were systematically compared with the data of PCL-based electrospun scaffolds previously used for soft tissue repair (Table 1). In conclusion, we have selected a PCL/GEL (7:3) composite incorporated with MMC and proceeded to conduct subsequent cellular experiments and animal studies.

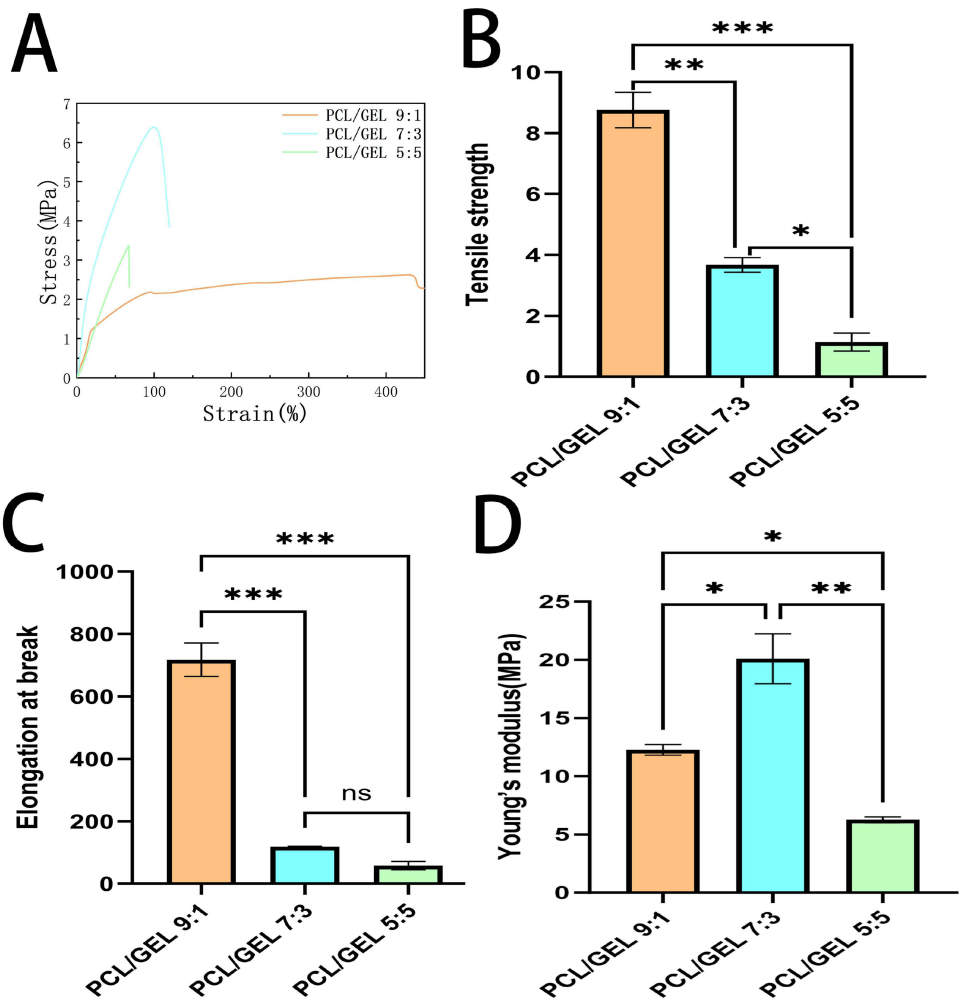


**Figure 4** Mechanical properties of PCL/GEL nanofibers: stress-strain curve (**A**), tensile strength (**B**), elongation at break (**C**), and Young's modulus (**D**) (*$P$-value < 0.05, **$P$-value < 0.01, ***$P$-value < 0.001, ns $P$-value > 0.05).


https://doi.org/10.2147/IJN.S574989

**Table 1** The Comparison of the Mechanical Properties of the Materials in This Study with Those of PCL-based Electrospun Scaffolds Previously Used for Soft Tissue Repair

| Material | Application Objectives | Tensile Strength (MPa) | Elongation at Break (%) | Young's Modulus (MPa) | Test Conditions | Reference |
|---|---|---|---|---|---|---|
| PCL/GEL (9:1) | Bladder repair | 8.75±0.2 | 712.91 ± 3.1 | 12.41±2.6 | Wet state | This work |
| PCL/GEL (7:3) | | 3.84 ± 0.5 | 118.42 ± 4 | 19.50 ± 4.6 | | |
| PCL/GEL (5:5) | | 1.12±0.3 | 52.27 ± 2.5 | 6.23±1.7 | | |
| PCL/Collagen | Skin regeneration | ~1.0–3.0 | ~80-180 | ~5-40 | Dry state | Powell HM et al, 2009[36] |
| PCL/GEL (High Orientation) | Skin regeneration | 14.7 ± 3.1 | 47 ± 11 | 179 ± 37 | Dry state | Chong EJ et al, 2007[10] |
| PCL/Chitosan | Bone regeneration | Not tested | Not tested | Not tested | Dry state | Dixon DT et al, 2025[25] |

One limitation of this study is that a comprehensive physical characterization (such as SEM, contact angle, and mechanical testing) of the MMC-loaded nanofibers was not conducted. Based on the completely consistent preparation process parameters, we inferred that their morphology was similar to that of the blank fibers, and we believe that the loading of MMC at such a low concentration has a negligible impact on the macroscopic material properties. Future studies will conduct more systematic parallel comparisons in material characterization to completely rule out the potential influence of material property changes on biological results.

## FTIR Spectroscopy Analysis

Fourier-transform infrared spectroscopy (FTIR) was employed to detect characteristic functional group peaks in the PCL/GEL and PCL/GEL/MMC composite materials. The spectra reveal that gelatin displays clear absorption bands at 1532 $cm^{-1}$ (amide II, N–H bending), 1635 $cm^{-1}$ (amide I, C=O stretching), and 3285 $cm^{-1}$ (N–H stretching). In comparison, PCL exhibits signature peaks at 1727 $cm^{-1}$ (C=O stretching), 2871 $cm^{-1}$ (symmetric C–H stretching), and 2948 $cm^{-1}$ (asymmetric C–H stretching) (Figure 5A). Furthermore, MMC shows distinct absorbance peaks at 1727 $cm^{-1}$ (carbonyl C=O stretching) and 3313 $cm^{-1}$ (O–H stretching) (Figure 5B). These FTIR results verify the

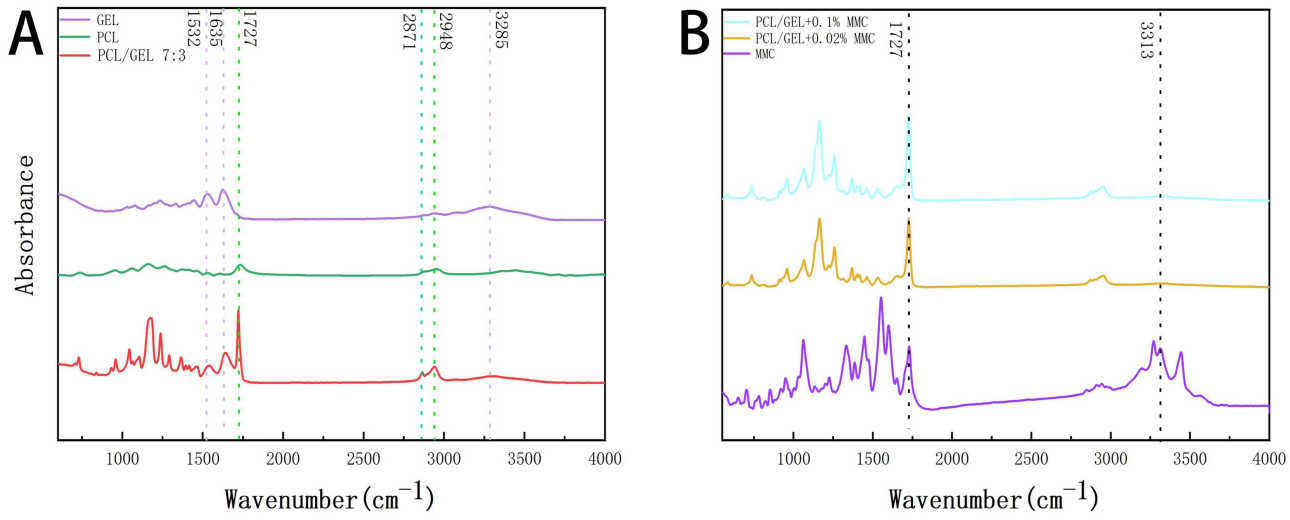


**Figure 5** Fourier Transform Infrared (FTIR) Spectroscopy Spectra: (**A**) GEL, PCL, PCL/GEL; (**B**) PCL/GEL + 0.1%MMC/0.02% MMC.


https://doi.org/10.2147/IJN.S574989

effective integration of MMC into the PCL/GEL nanofibrous matrix while maintaining the fundamental chemical integrity of the scaffold.

## Investigation of Drug Release

As illustrated in Figure 6, MMC demonstrated a sustained release characteristic from the nanofiber membranes. In the case of the PCL/GEL/0.1% MMC nanofiber membrane, an initial burst release of the drug was observed within the first three days, followed by a stable and continuous release phase. This culminated in a cumulative release of 95% by day eight. Similarly, the PCL/GEL/0.02% MMC nanofiber membrane exhibited a burst release behavior during the first four days, after which it transitioned into a stable release phase. By day eight, it achieved an identical cumulative release rate of 95% (Figure 6). The initial rapid release of MMC is mainly due to the diffusion of drug molecules located on the surface of the matrix. In contrast, the subsequent sustained release is a result of gradual degradation induced by interactions between the drug and the polymer matrix. The cumulative release profiles of MMC under different drug loading levels (0.02% and 0.1%) display highly similar kinetic patterns, particularly during the initial burst release phase and the subsequent plateau stage. This observation suggests that, within the tested concentration range, the release kinetics are predominantly governed by the intrinsic properties of the carrier material, rather than being sensitive to variations in drug loading.

## Biocompatibility of Nanofiber Membranes

An optimal scaffold material intended for the replacement or enhancement of the bladder wall should demonstrate exceptional biocompatibility to reduce inflammation and mitigate foreign body reactions associated with transplantation.[37] MMC undergoes intricate biological reduction processes within the body, leading to the formation of interstrand crosslinks (ICLs). This may lead to mitotic arrest and subsequent cell death, ultimately causing cytotoxic damage.[38] To assess the biocompatibility of the nanofiber scaffold, we conducted co cultivation of various nanofiber membranes with SMCs and ECs (Figure 7A–F).

As illustrated in Figure 7G and H), cell proliferation was evaluated on days 1, 3, and 7 using the CCK-8 assay in the PCL/GEL, PCL/GEL/0.02% MMC, and PCL/GEL/0.1% MMC groups. A marked time-dependent rise in optical density (OD) values was observed across all scaffold groups. Moreover, the OD values of all fiber membrane groups were markedly higher than those observed in the control group. This indicates that SMCs and ECs possess the ability to survive and proliferate effectively on these fibrous membranes. It is noteworthy that among the three types of nanofiber scaffolds, SMCs and ECs exhibited the highest OD values in the PCL/GEL group. In contrast, the lowest OD values were recorded in the PCL/GEL/0.1% MMC group. A statistically significant difference was found for SMCs. However, no

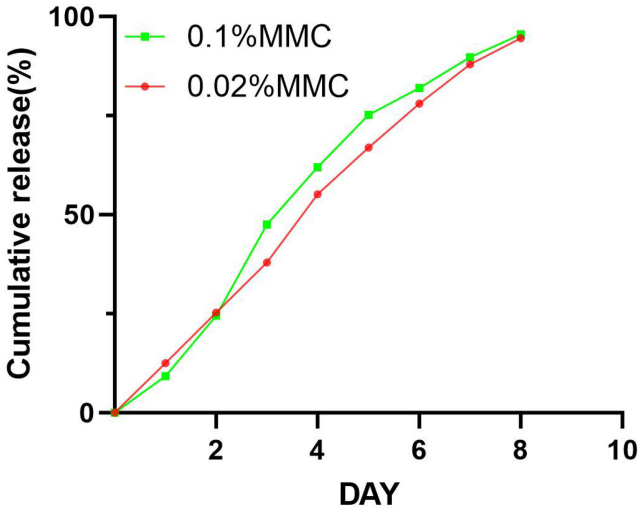


**Figure 6** Cumulative drug release from PCL/GEL/0.1% MMC nanofiber membrane and PCL/GEL/0.02% MMC nanofiber membrane at 37 °C.

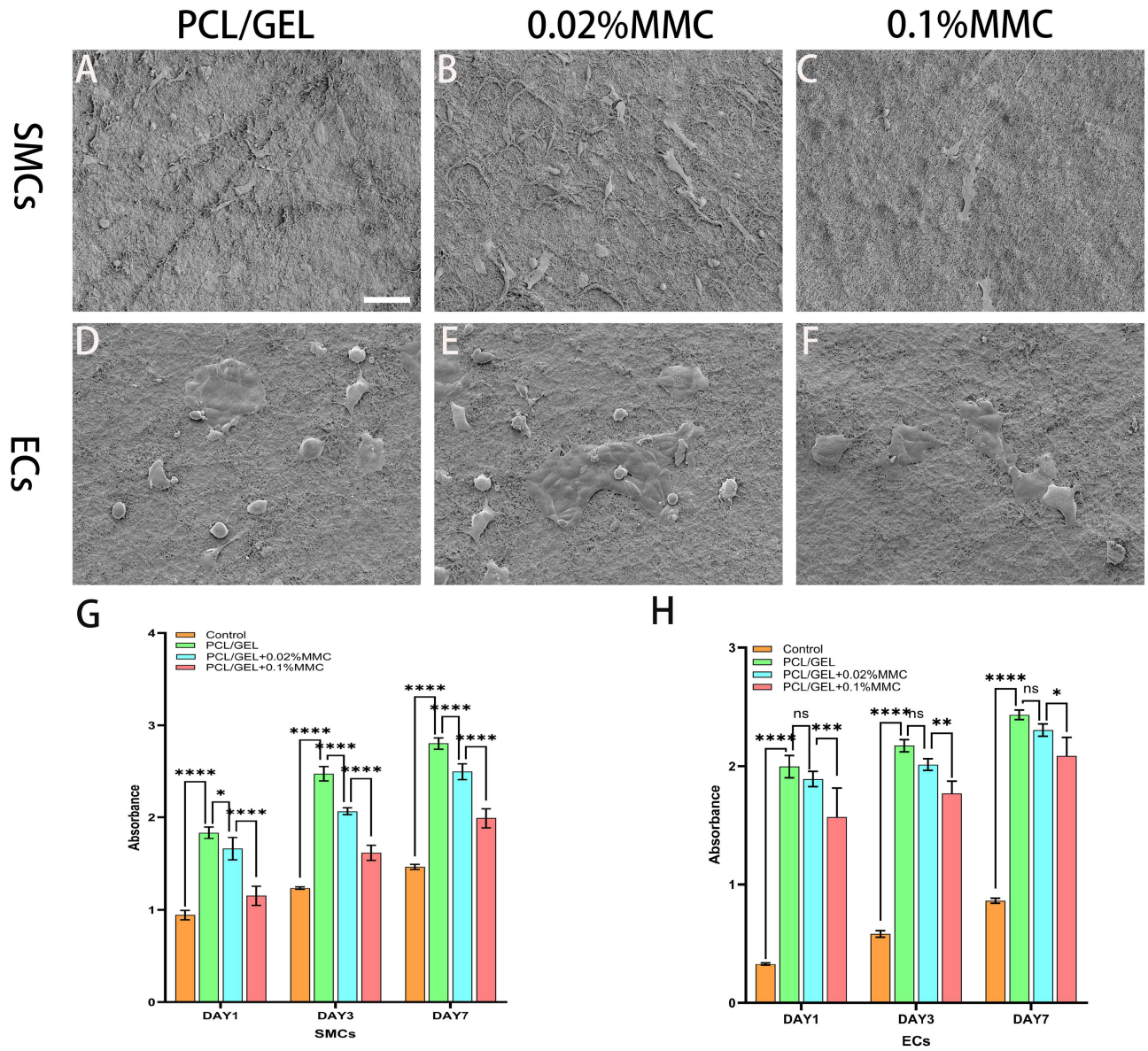


**Figure 7** SMCs and ECs were seeded onto the nanofiber membranes after 72 hours (**A**–**F**) (scale bar = 20 μm). The cell viability of SMCs and ECs on each nanofiber membrane was assessed using the CCK-8 assay (**G** and **H**) (**P*-value < 0.05, ***P*-value < 0.01, ****P*-value < 0.001, *****P*-value < 0.0001, ns *P*-value > 0.05).

statistical differences were observed for ECs on low-concentration MMC nanofiber scaffolds. This suggested that MMC exhibited a certain level of cytotoxicity towards these two cell types, however, PCL/GEL/0.02% MMC appeared to be relatively safe. SEM analysis further revealed that cells grown on the PCL/GEL, PCL/GEL/0.02% MMC, and PCL/GEL/0.1% MMC nanofiber surfaces maintained typical and well-preserved morphological features.

To assess the capacity of PCL/GEL/MMC nanofiber membranes to direct epithelial cells and SMCs toward the development of aligned, anisotropic tissue structures, immunofluorescence staining was conducted to examine the expression of α-SMA, a critical marker of smooth muscle contractile function, and keratin (AE1/AE3), a key epithelial cell surface protein. As shown in Figure 8, all nanofiber groups exhibited positive immunostaining for both α-SMA and AE1/AE3. However, when compared to the PCL/GEL group, the PCL/GEL/MMC groups showed a modest decrease in the expression levels of both α-SMA and keratin (AE1/AE3). However, they remained higher than those observed in the control group. These findings suggested that PCL/GEL/MMC can enhance the expression of actin in SMCs and ECs, demonstrated good cell compatibility. Notably, the expression level of PCL/GEL/0.02% MMC exceeded that of PCL/


https://doi.org/10.2147/IJN.S574989

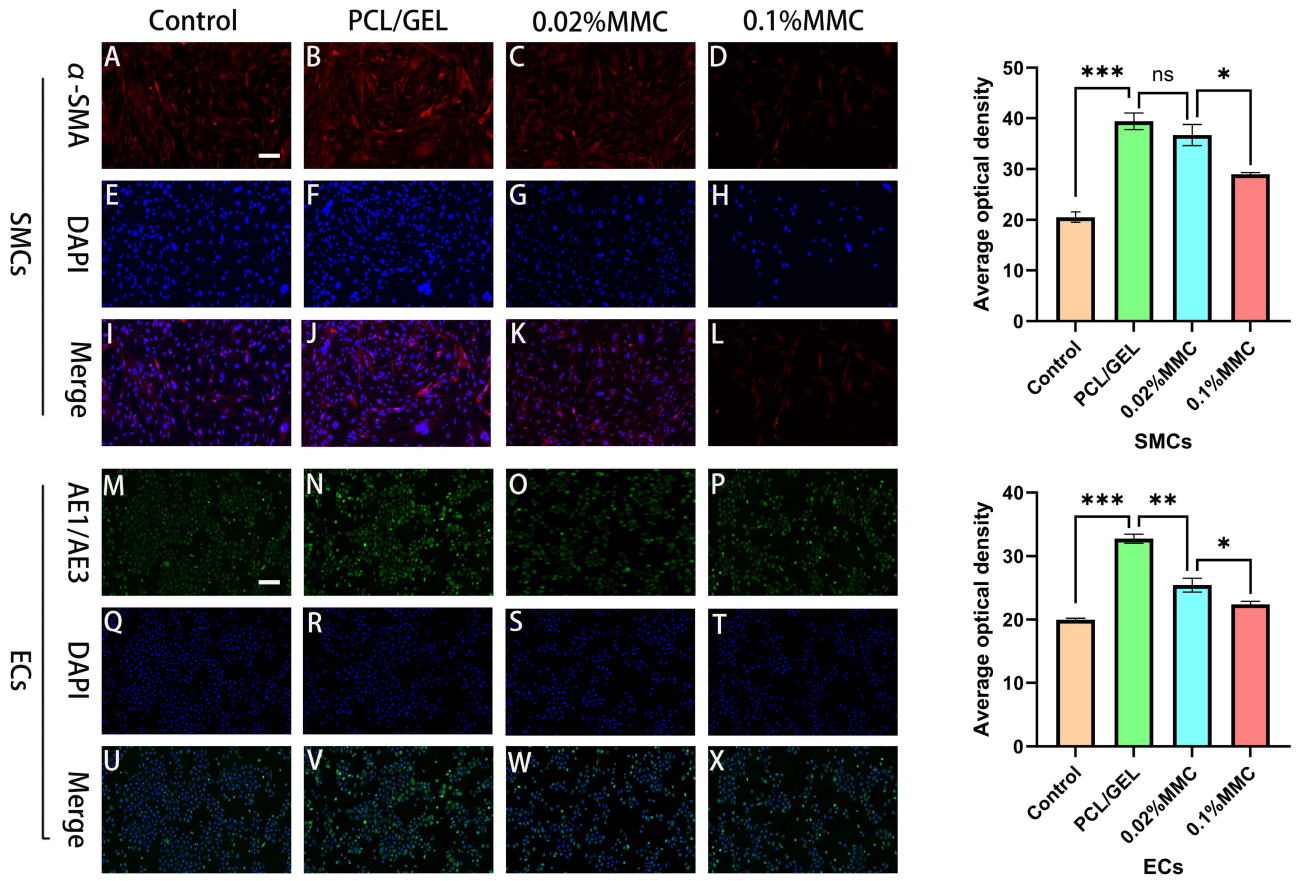


**Figure 8** In vitro cell phenotype expression. 72 hours post-vaccination, SMCs were subjected to immunofluorescence staining for actin (α-SMA, red) and the cell nucleus (blue) (**A**–**L**). ECs on the nanofiber membrane were similarly stained using immunofluorescence techniques for keratin (AE1/AE3, green) and the cell nucleus (blue) (**M**–**X**). (scale bar=20 microns) (ns. indicates no significant difference).

GEL/0.1% MMC, suggested that the PCL/GEL/0.02% MMC nanofiber material exhibits superior cell compatibility. For the forthcoming animal experiments, we have selected PCL/GEL and PCL/GEL/0.02% MMC materials, which are distinguished by their relatively high safety profile for research purposes.

## Animal Experiments

The selection of rats and the animal experimental procedures were conducted as previously described. A midline abdominal incision was performed to expose the rat bladder and create a defect model. Using 5–0 absorbable sutures, appropriately sized PCL/GEL and PCL/GEL/0.02% MMC nanofiber membranes were implanted into the defect site utilizing intermittent suturing techniques (Figure 9A–C). Furthermore, urinary catheters were retained in place for the rats following surgery.

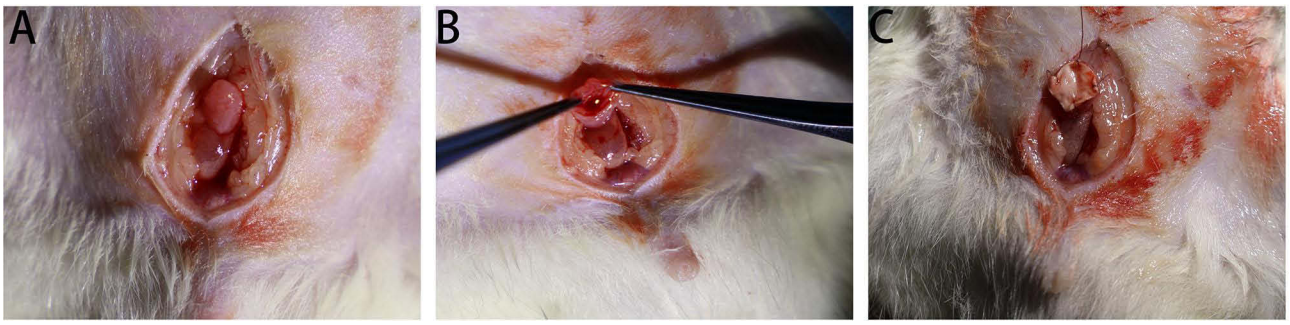


**Figure 9** Establishment of a rat bladder defect model and the implantation of nanofiber materials into the defect site through intermittent suturing (**A**–**C**).

With the exception of two rats that unfortunately succumbed to infection on the second and third days post-surgery due to catheter dislodgement, all other rats survived throughout the duration of the experimental period. To assess the repair of bladder defects in a rat model after implantation of the nanofiber membrane, retrograde cystography was conducted on all animals at 12 weeks following surgery. The results of retrograde cystography indicated no obstruction in the urethra across all three groups of rats, with clear delineation of bladder contours. However, in the PCL/GEL group, some rats exhibited thicker bladder walls, which may be attributed to fibrosis and scar formation during the process of bladder defect repair (Figure 10A–C). Although no stone formation was observed in the bladders of experimental rats in this study, the surfaces of hydrophobic polymers such as PCL have been consistently demonstrated in multiple studies to promote protein adsorption and crystal nucleation, with evidence of calculi development reported in animal urinary tract models.[39] To address this potential risk, future studies will establish a long-term observation period exceeding six months, during which serial X-ray radiography will be performed to specifically monitor for stone formation. Furthermore, surface hydrophilic modification of the fibrous scaffold will be implemented to construct a bioinert interface that resists protein fouling and crystal deposition, thereby fundamentally mitigating the risk of urolithiasis.

## Histopathological Staining and Immunohistochemical Analysis

To further elucidate the repair status of the rat bladder, we assessed the overall morphology of the bladder following a two-month period of repair, employing HE and Masson staining techniques. Our findings revealed that the PCL/GEL group displayed an irregular and discontinuous epithelial layer, along with substantial collagen accumulation on the surface of the regenerated bladder tissue (Figure 11A–F). In contrast, the PCL/GEL/0.02% MMC group demonstrated a well-organized and continuous epithelial layer in the submucosal tissue of the bladder, closely resembling that of the control group. This was accompanied by notable collagen deposition.

Sirius Red staining was conducted to assess the organization and spatial distribution of collagen fibers in the regenerated bladder tissue (Figure 11G–L). Under this staining method, type III collagen is visualized as green, while type I collagen is identified by red or yellow hues.[40] Notably, type III collagen is the major subtype present in hypertrophic scar tissue.[41] The results indicated that in the PCL/GEL group, there was a greater deposition of type III collagen accompanied by a reduced presence of type I collagen, which resulted in an increased green area. Conversely, the PCL/GEL/0.02% MMC group exhibited a predominant deposition of type I collagen, which appeared a bright yellow and resembled the collagen distribution observed in the control group. This observation indicates that the collagen fibers newly generated in this group exhibit a composition similar to that of native bladder tissue.

Histological analysis at 12 weeks post-operation revealed the absence of an identifiable, intact original fibrous membrane structure within the implantation site. This observation indicates that the PCL/GEL scaffold has undergone substantial biodegradation, with newly formed tissue having fully occupied the defect region and achieved seamless integration with the surrounding host tissue. The scaffold served three primary functions: first, it provided temporary mechanical support to prevent defect collapse and maintain bladder structural integrity; second, it guided organized tissue regeneration, where its nanotopographical cues and anti-fibrotic microenvironment promoted the development of

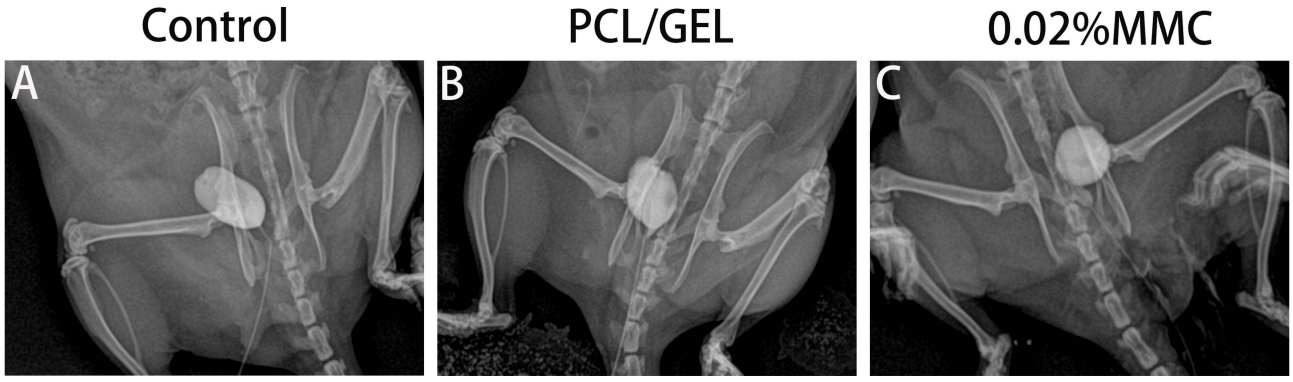


**Figure 10** Bladder imaging of the control group, PCL/GEL group, and PCL/GEL/0.02% MMC group rats was conducted 12 weeks post-surgery (**A**–**C**).


https://doi.org/10.2147/IJN.S574989

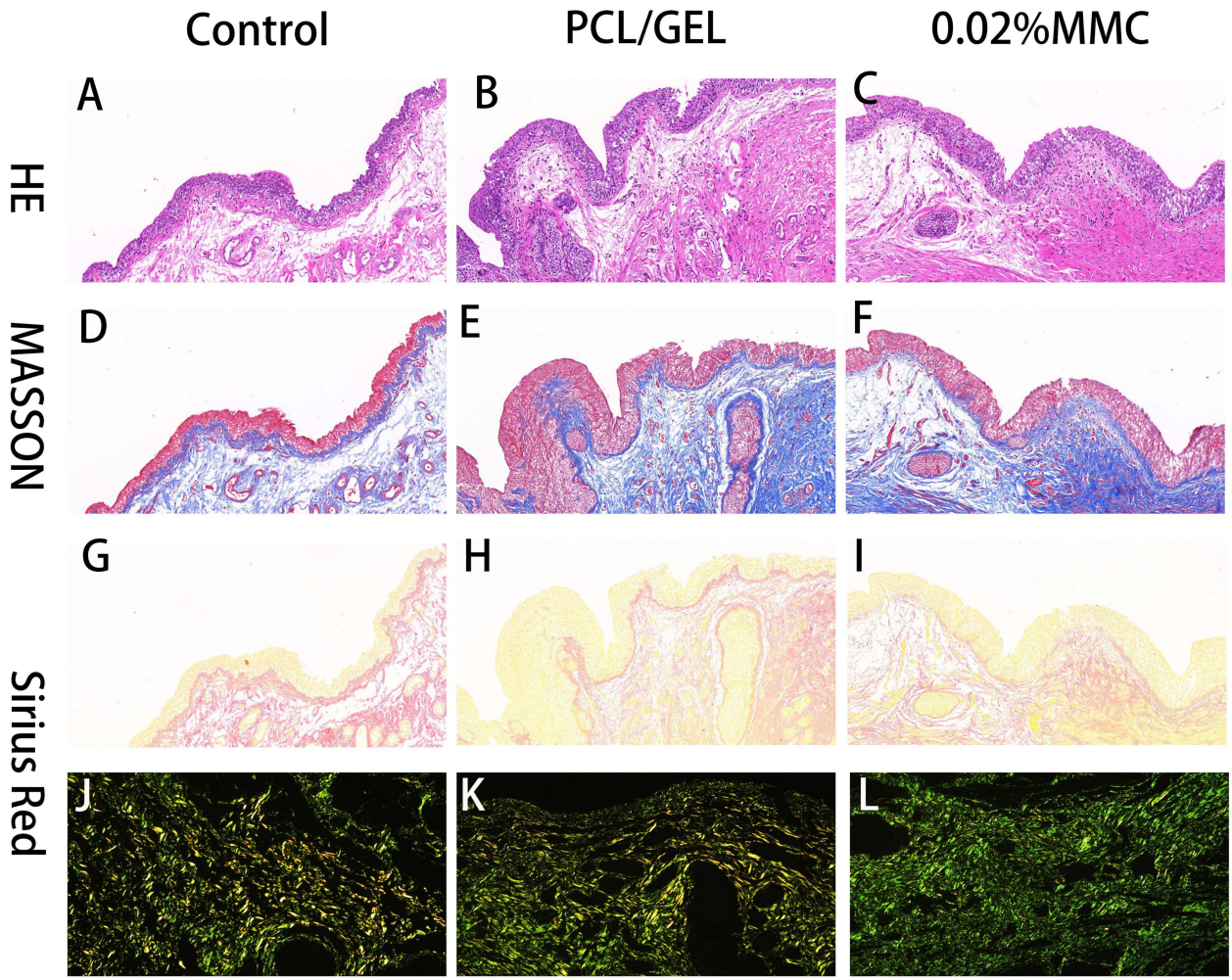


**Figure 11** Histopathological analysis was performed on nanofiber membranes implanted in rats. Hematoxylin and eosin (HE) staining (**A**–**C**), Masson's trichrome staining (**D**–**F**), and Sirius Red staining (**G**–**L**) were carried out using both bright-field and polarized light microscopy (**J**–**L**) to assess the regenerated bladder tissue in each group two months after surgery. (Scale bar: 50 μm).

functional tissues—such as epithelium and smooth muscle—over fibrotic scar formation; third, through progressive degradation, the scaffold fulfilled its regenerative role and was ultimately replaced by native-like tissue. These combined effects contributed to the recovery of key bladder functions, including capacity, compliance, and contractility.

The formation of new blood vessels is essential for effective wound repair and the recovery of normal bladder tissue function. CD31 is a key protein that serves as an important marker for assessing tissue angiogenesis.[42] To determine the localization and expression of CD31, bladder specimens underwent immunohistochemical analysis to assess the angiogenic response in bladder repair tissue (Figure 12A–C). The findings from the semi-quantitative analysis revealed that, after a two-month period, the PCL/GEL/0.02% MMC group demonstrated significantly enhanced neovascularization in comparison to the PCL/GEL group (Figure 12J). In addition, recent studies have shown that the physicochemical properties of tissue engineering scaffolds can actively regulate the polarization of immune cells such as macrophages towards a pro-regenerative (M2) phenotype, thereby secreting a series of pro-angiogenic factors (such as VEGF, PDGF-BB), and creating a microenvironment conducive to vascularization.[43]

TGF-β is a widely recognized cytokine that promotes fibrosis. Upon tissue damage, its secretion increases in the fibrotic milieu, activating SMAD2/3 via binding to TGF-β receptor 1 and 2 (TGFBR1/2). Once phosphorylated, SMAD2/3 migrates into the nucleus and drives the transcription of extracellular matrix proteins by directly regulating key downstream genes, including PAI1, CTGF, and c-Jun.[44] Numerous prospective randomized studies have established that

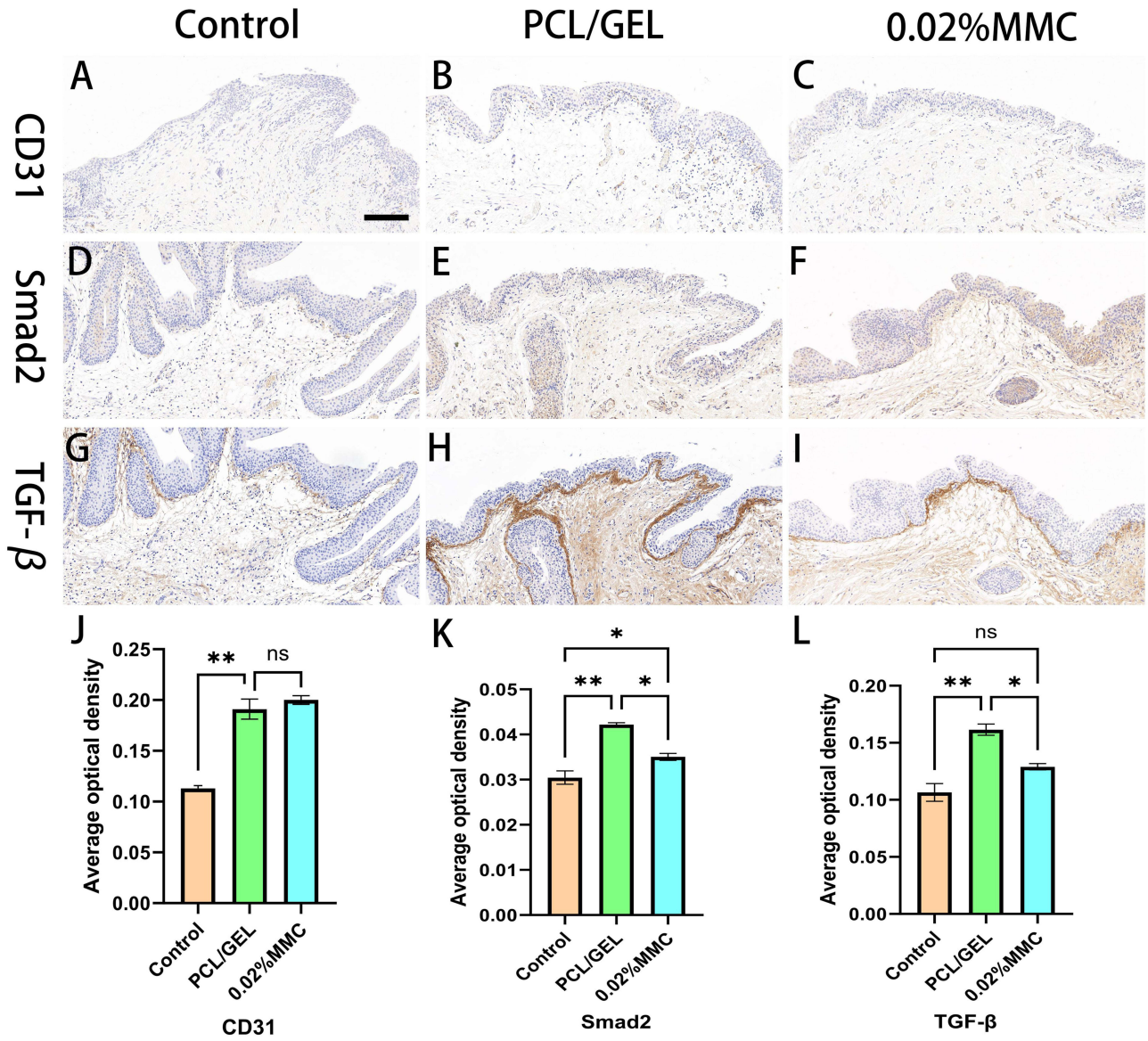


**Figure 12** Immunohistochemical staining analysis of nanofiber membranes implanted in rats was conducted. CD31 staining (**A**–**C**), Smad2 staining (**D**–**F**), and TGF-β staining (**G**–**I**) were performed on bladder repair tissues from each group 2 months post-surgery (Scale bar: 50μm). The average optical density for CD31 (**J**), Smad2 (**K**), and TGF-β (**L**) (**P*-value < 0.05, ***P*-value < 0.01, ns *P*-value > 0.05).

MMC effectively regulates the TGF-β/Smad signaling cascade and inhibits scar development.[45,46] To investigate whether PCL/GEL/0.02% MMC attenuates postoperative bladder fibrosis in rats by targeting the TGF-β/Smad pathway, we examined the expression of TGF-β and Smad2 in tissue samples (Figure 12D–I). Immunohistochemical analysis showed markedly lower levels of TGF-β and Smad2 in the PCL/GEL/0.02% MMC group compared to the PCL/GEL group. These observations were further supported by semi-quantitative evaluation, which revealed a statistically significant reduction in the mean optical density of both TGF-β and Smad2 in the PCL/GEL/0.02% MMC group relative to the PCL/GEL group (Figure 12K and L). Notably, the mean optical density values in the PCL/GEL/0.02% MMC group were comparable to those in the control group. Collectively, these results suggest that MMC mediates its anti-fibrotic effect through suppression of the TGF-β/Smad signaling pathway.


https://doi.org/10.2147/IJN.S574989

## Conclusion

This study successfully developed a mitomycin C (MMC)-loaded PCL/GEL composite nanofiber membrane for the repair of bladder defects and the prevention of postoperative fibrosis. The optimized PCL/Gel ratio (7:3) combined with electrospinning yielded uniform nanofibers with an average diameter of approximately 612 nm, a dimension that closely mimics the topological features of the natural extracellular matrix (ECM). This biomimetic architecture significantly enhanced the adhesion and proliferation of both bladder epithelial cells and smooth muscle cells. Under wet conditions, the membrane demonstrated moderate mechanical properties well-suited for soft tissue applications, with values comparable to those reported for established skin regeneration scaffolds, such as PCL/collagen constructs. Furthermore, the sustained yet rapid release profile of MMC fulfilled the critical therapeutic window required for early-stage anti-fibrotic intervention following surgical implantation. Collectively, these findings demonstrate that the engineered scaffold integrates structural biomimicry, mechanical compatibility, and localized pharmacological functionality in a single platform, representing a promising strategy for bladder tissue regeneration.

This study validates and extends the established paradigms of "material synergy" and "structural biomimicry" in tissue engineering. First, the PCL/GEL system employed in this work demonstrates a well-defined synergistic effect—PCL provides a robust mechanical framework while gelatin imparts bioactive cues—consistent with conclusions from recent comprehensive reviews.[19] Second, the optimized PCL/GEL (7:3) formulation and electrospinning parameters yielded nanofibers with an average diameter of approximately 612 nm, which falls within the widely recognized "ideal topological range" associated with enhanced cellular responses.[29] This structural fidelity to native extracellular matrix architecture provides a mechanistic explanation for the observed superior cell compatibility. In contrast to prior studies, the present work uniquely applies this validated biomaterial platform to bladder tissue repair—a site characterized by complex dynamic mechanical demands—and further integrates it with localized delivery of mitomycin C (MMC) to mitigate fibrosis. When compared to existing strategies summarized in current bladder tissue engineering reviews,[47] our approach represents a multifunctional, integrated solution that concurrently delivers structural support (via PCL), instructive topographical signals (via GEL fiber architecture), and pharmacological intervention (via MMC), thereby advancing the functional design of regenerative scaffolds.

Although this study yielded promising results, several limitations remain that highlight important directions for future research. First, comprehensive physical characterization of the MMC-loaded nanofibers—including morphological analysis by scanning electron microscopy (SEM), surface wettability via contact angle measurement, and mechanical testing—was not performed. Given the identical fabrication parameters used for both loaded and blank fibers, we reasonably infer that the fiber morphology remains comparable, and that the incorporation of a low concentration of MMC has a negligible impact on the macroscopic properties of the scaffold. Second, this study preliminarily observed, via immunohistochemistry, a reduction in the expression levels of TGF-β and Smad2 within the implantation site of the MMC-loaded scaffold, suggesting that MMC may exert its anti-fibrotic effect through modulation of the TGF-β/Smad signaling pathway. However, we acknowledge that semi-quantitative IHC analysis alone is insufficient for precise quantification of key protein expression changes in this pathway. To definitively confirm the molecular mechanism underlying MMC's inhibition of fibrotic signaling, future studies should employ Western Blot to quantify TGF-β, Smad2, and downstream effector proteins in the regenerated tissue, combined with qPCR to assess the transcriptional levels of associated genes. Such complementary approaches are essential for establishing a robust mechanistic foundation. Third, this study primarily relied on histomorphological analyses (including H&E and Masson's trichrome staining) and static imaging modalities—specifically retrograde cystography—to evaluate the structural outcomes of bladder repair. While these methods effectively demonstrate tissue architecture and morphological integrity, urodynamic assessment remains the gold standard for evaluating functional parameters such as bladder compliance, storage-phase stability, and detrusor contractility during voiding. Notably, this study did not include quantitative evaluation of critical functional metrics, including pressure–volume relationships during bladder filling (compliance), leak point pressure, maximum cystometric capacity, or detrusor contractile strength. Furthermore, the regeneration of neural innervation within the regenerated bladder tissue was not investigated. A fully functional neobladder requires not only the regeneration of smooth muscle and urothelium but also the precise reestablishment of both intrinsic ganglia and extrinsic neural circuits to coordinate

physiological micturition reflexes. The PCL/GEL/MMC scaffold employed in this work was primarily designed to mitigate fibrosis and guide cellular ingrowth, without incorporating specific strategies to promote neural regeneration. Future iterations of this scaffold could be advanced into a "neuroregenerative intelligent scaffold" through the integration of neurotrophic cues or conductive biomaterials, thereby enabling more comprehensive restoration of bladder function.

The wet-state Young's modulus measured in this study is indeed substantially higher than that of native bladder tissue. This "mechanical mismatch" represents a prevalent challenge for most synthetic polymer-based scaffolds when applied to dynamic soft tissues. An excessively high modulus may induce local stress shielding, impair mechanotransduction, and potentially promote chronic inflammatory responses. To address this limitation, future material optimization strategies should focus on intrinsically reducing the macroscopic stiffness through the incorporation of flexible segments (eg, PEG), increased blending ratios with hydrophilic components such as gelatin, or the design of interpenetrating polymer networks. These approaches aim to enhance bulk compliance while preserving microstructural integrity, thereby improving biomechanical compatibility. A central direction for future research is to functionally modify the PCL/GEL nanofiber platform developed in this study—through strategies such as grafting specific peptide sequences, incorporating exosomes, or enabling controlled cytokine release—to precisely regulate the recruitment, homing, proliferation, and directed differentiation of endogenous stem or progenitor cells. Such advancements would drive a critical transition in tissue engineering materials toward achieving both functional and structural regeneration.

## Acknowledgments

The author would like to extend heartfelt gratitude to the Human Anatomy Experimental Training Center at the School of Basic Medical Sciences, Wannan Medical College.

## Author Contributions

All authors made a significant contribution to the work reported, whether that is in the conception, study design, execution, acquisition of data, analysis and interpretation, or in all these areas; took part in drafting, revising or critically reviewing the article; gave final approval of the version to be published; have agreed on the journal to which the article has been submitted; and agree to be accountable for all aspects of the work.

## Funding

This research was funded by the scientific research fund for young and middle-aged scholars of Wannan Medical College (NO. WK2023ZQNZ37 and NO. WK2024ZQNZ58), Anhui Provincial Department of Education Scientific Research Project (NO.2025AHGXZK31509) and Anhui Provincial Department of Education Key Research Project Fund for Universities in 2023 (NO. 2023AH051728).

## Disclosure

The authors declare no known competing interests in this study.

## References

1. Jayarajah U, Gunawardene M, Willaraarachchi M, et al. Clinical characteristics and outcome of genitourinary tuberculosis in Sri Lanka: an observational study. *BMC Infect Dis*. 2021;21(1):1279. doi:10.1186/s12879-021-06990-z
2. Cheng PJ, Myers JB. Augmentation cystoplasty in the patient with neurogenic bladder. *World J Urol*. 2020;38(12):3035–3046. doi:10.1007/s00345-019-02919-z
3. Queissert F, Bruecher B, van Ophoven A, Schrader AJ. Supratrigonal cystectomy and augmentation cystoplasty with ileum or ileocecum in the treatment of ulcerative interstitial cystitis/bladder pain syndrome: a 14-year follow-up. *Int Urogynecol J*. 2022;33(5):1267–1272. doi:10.1007/s00192-022-05110-y
4. Kim S, Buckley JC. Robotic lower urinary tract reconstruction. *Urol Clin North Am*. 2021;48(1):103–112. doi:10.1016/j.ucl.2020.09.006
5. Ninan N, Thomas S, Grohens Y. Wound healing in urology. *Adv Drug Deliv Rev*. 2015;82–83:93–105. doi:10.1016/j.addr.2014.12.002
6. Di XP, Jin X, Ai JZ, et al. YAP/Smad3 promotes pathological extracellular matrix microenviroment-induced bladder smooth muscle proliferation in bladder fibrosis progression. *MedComm*. 2022;3(4):e169. doi:10.1002/mco2.169
7. Zamani M, Shakhssalim N, Ramakrishna S, Naji M. Electrospinning: application and prospects for urologic tissue engineering. *Front Bioeng Biotechnol*. 2020;8:579925. doi:10.3389/fbioe.2020.579925

8. Zheng Q, Xi Y, Weng Y. Functional electrospun nanofibers: fabrication, properties, and applications in wound-healing process. *RSC Adv*. 2024;14(5):3359–3378. doi:10.1039/d3ra07075a
9. Gautam S, Sharma C, Purohit SD, et al. Gelatin-polycaprolactone-nanohydroxyapatite electrospun nanocomposite scaffold for bone tissue engineering. *Mater Sci Eng C Mater Biol Appl*. 2021;119:111588. doi:10.1016/j.msec.2020.111588
10. Silva JC, Udangawa RN, Chen J, et al. Kartogenin-loaded coaxial PGS/PCL aligned nanofibers for cartilage tissue engineering. *Mater Sci Eng C Mater Biol Appl*. 2020;107:110291. doi:10.1016/j.msec.2019.110291
11. Eldurini S, Abd El-Hady BM, Shafaa MW, Gad AAM, Tolba E. A multicompartment vascular implant of electrospun wintergreen oil/polycaprolactone fibers coated with poly(ethylene oxide). *Biomed J*. 2021;44(5):589–597. doi:10.1016/j.bj.2020.04.008
12. Heidari M, Bahrami SH, Ranjbar-Mohammadi M, Milan PB. Smart electrospun nanofibers containing PCL/gelatin/graphene oxide for application in nerve tissue engineering. *Mater Sci Eng C Mater Biol Appl*. 2019;103:109768. doi:10.1016/j.msec.2019.109768
13. Han X, Zhao M, Xu R, et al. Electrospun hyaluronan nanofiber membrane immobilizing aromatic doxorubicin as therapeutic and regenerative biomaterial. *Int J Mol Sci*. 2023;24(8):7023. doi:10.3390/ijms24087023
14. Adamowicz J, Pokrywczyńska M, Tworkiewicz J, et al. New amniotic membrane based biocomposite for future application in reconstructive urology. *PLoS One*. 2016;11(1):e0146012. doi:10.1371/journal.pone.0146012
15. Xie L, Cheng L, Wei Y. Mitomycin C enhanced the antitumor efficacy of Rocaglamide in colorectal cancer. *Pathol Res Pract*. 2023;243:154350. doi:10.1016/j.prp.2023.154350
16. Uyeturk U, Gucuk A, Firat T, Kemahli E, Kukner A, Ozyalvacli ME. Effect of mitomycin, bevacizumab, and 5-Fluorouracil to inhibit urethral fibrosis in a rabbit model. *J Endourol*. 2014;28(11):1363–1367. doi:10.1089/end.2014.0420
17. Ramírez-Ruiz F, Núñez-Tapia I, Piña-Barba MC, Alvarez-Pérez MA, Guarino V, Serrano-Bello J. Polycaprolactone for hard tissue regeneration: scaffold design and in vivo implications. *Bioengineering*. 2025;12(1). doi:10.3390/bioengineering12010046
18. Zhang YZ, Venugopal J, Huang ZM, Lim CT, Ramakrishna S. Characterization of the surface biocompatibility of the electrospun PCL-collagen nanofibers using fibroblasts. *Biomacromolecules*. 2005;6(5):2583–2589. doi:10.1021/bm050314k
19. Sell SA, McClure MJ, Garg K, Wolfe PS, Bowlin GL. Electrospinning of collagen/biopolymers for regenerative medicine and cardiovascular tissue engineering. *Adv Drug Deliv Rev*. 2009;61(12):1007–1019. doi:10.1016/j.addr.2009.07.012
20. Chong EJ, Phan TT, Lim IJ, et al. Evaluation of electrospun PCL/gelatin nanofibrous scaffold for wound healing and layered dermal reconstitution. *Acta Biomater*. 2007;3(3):321–330. doi:10.1016/j.actbio.2007.01.002
21. Schnell E, Klinkhammer K, Balzer S, et al. Guidance of glial cell migration and axonal growth on electrospun nanofibers of poly-epsilon-caprolactone and a collagen/poly-epsilon-caprolactone blend. *Biomaterials*. 2007;28(19):3012–3025. doi:10.1016/j.biomaterials.2007.03.009
22. Zhao L, Xia J, Yang C, et al. Poly(L-lactic acid)/gelatin microfiber membrane loaded with mitomycin C promoting bladder defect repair by anti-fibrosis and antibacterial action. *J Mater Chem B*. 2025;13(18):5427–5439. doi:10.1039/d4tb02521k
23. Govindaraju DT, Kao HH, Chien YM, Chen JP. Composite polycaprolactone/gelatin nanofiber membrane scaffolds for mesothelial cell culture and delivery in mesothelium repair. *Int J Mol Sci*. 2024;25(18):9803. doi:10.3390/ijms25189803
24. Sivaraman S, Amoroso N, Gu X, et al. Evaluation of Poly (Carbonate-Urethane) urea (PCUU) scaffolds for urinary bladder tissue engineering. *Ann Biomed Eng*. 2019;47(3):891–901. doi:10.1007/s10439-018-02182-0
25. Kao HH, Kuo CY, Tagadur govindaraju D, Chen KS, Chen JP. Polycaprolactone/chitosan composite nanofiber membrane as a preferred scaffold for the culture of mesothelial cells and the repair of damaged mesothelium. *Int J Mol Sci*. 2022;23(17):9517. doi:10.3390/ijms23179517
26. Tuanchai A, Iamphring P, Suttaphakdee P, et al. Bilayer scaffolds of PLLA/PCL/CAB ternary blend films and curcumin-incorporated PLGA electrospun nanofibers: the effects of polymer compositions and solvents on morphology and molecular interactions. *Polymers*. 2024;16(12):1679. doi:10.3390/polym16121679
27. Pham QP, Sharma U, Mikos AG. Electrospinning of polymeric nanofibers for tissue engineering applications: a review. *Tissue Eng*. 2006;12(5):1197–1211. doi:10.1089/ten.2006.12.1197
28. Song JH, Kim HE, Kim HW. Production of electrospun gelatin nanofiber by water-based co-solvent approach. *J Mater Sci Mater Med*. 2008;19(1):95–102. doi:10.1007/s10856-007-3169-4
29. Christopherson GT, Song H, Mao HQ. The influence of fiber diameter of electrospun substrates on neural stem cell differentiation and proliferation. *Biomaterials*. 2009;30(4):556–564. doi:10.1016/j.biomaterials.2008.10.004
30. Lutolf MP, Hubbell JA. Synthetic biomaterials as instructive extracellular microenvironments for morphogenesis in tissue engineering. *Nat Biotechnol*. 2005;23(1):47–55. doi:10.1038/nbt1055
31. Loyo C, Cordoba A, Palza H, et al. Effect of gelatin coating and GO incorporation on the properties and degradability of electrospun PCL scaffolds for bone tissue regeneration. *Polymers*. 2023;16(1):129. doi:10.3390/polym16010129
32. Liu Z, Chen X, Li C. Fabrication of a bionic asymmetric wettable Cu-doped chitosan-laponite-PCL wound dressing with rapid healing and antibacterial effect. *Biomed Mater*. 2022;17(5):055008. doi:10.1088/1748-605X/ac8130
33. Naseri M, Hedayatnazari A, Tayebi L. PGS/gelatin nanocomposite electrospun wound dressing. *J Compos Sci*. 2023;7(6):237. doi:10.3390/jcs7060237
34. Hanczar M, Moazen M, Day R. The significance of biomechanics and scaffold structure for bladder tissue engineering. *Int J Mol Sci*. 2021;22(23):12657. doi:10.3390/ijms222312657
35. Ajalloueian F, Lemon G, Hilborn J, Chronakis IS, Fossum M. Bladder biomechanics and the use of scaffolds for regenerative medicine in the urinary bladder. *Nat Rev Urol*. 2018;15(3):155–174. doi:10.1038/nrurol.2018.5
36. Powell HM, Boyce ST. Engineered human skin fabricated using electrospun collagen-PCL blends: morphogenesis and mechanical properties. *Tissue Eng Part A*. 2009;15(8):2177–2187. doi:10.1089/ten.tea.2008.0473
37. Sharma S, Basu B. Biomaterials assisted reconstructive urology: the pursuit of an implantable bioengineered neo-urinary bladder. *Biomaterials*. 2022;281:121331. doi:10.1016/j.biomaterials.2021.121331
38. Cheng SY, Delgado-Cruzata L, Clement CC, et al. Cytotoxicity, crosslinking and biological activity of three mitomycins. *Bioorg Chem*. 2022;123:105744. doi:10.1016/j.bioorg.2022.105744
39. Atala A, Bauer SB, Soker S, Yoo JJ, Retik AB. Tissue-engineered autologous bladders for patients needing cystoplasty. *Lancet*. 2006;367(9518):1241–1246. doi:10.1016/s0140-6736(06)68438-9
40. Gardeazabal L, Izeta A. Elastin and collagen fibres in cutaneous wound healing. *Exp Dermatol*. 2024;33(3):e15052. doi:10.1111/exd.15052

41. Kim HY, Im HY, Chang HK, et al. Correlation between collagen type I/III ratio and scar formation in patients undergoing immediate reconstruction with the round block technique after breast-conserving surgery. *Biomedicines*. 2023;11(4). doi:10.3390/biomedicines11041089
42. Li X, Liu R, Liu W, et al. Panax quinquefolium L. and salvia miltiorrhiza Bunge. Enhances angiogenesis by regulating the miR-155-5p/HIF-1α/VEGF axis in acute myocardial infarction. *Drug Des Devel Ther*. 2023;17:3249–3267. doi:10.2147/dddt.S426345
43. McWhorter FY, Wang T, Nguyen P, Chung T, Liu WF. Modulation of macrophage phenotype by cell shape. *Proc Natl Acad Sci U S A*. 2013;110(43):17253–17258. doi:10.1073/pnas.1308887110
44. Song Y, Wei J, Li R, et al. Tyrosine kinase receptor B attenuates liver fibrosis by inhibiting TGF-β/SMAD signaling. *Hepatology*. 2023;78(5):1433–1447. doi:10.1097/hep.0000000000000319
45. Wolters JEJ, van Mechelen RJS, Al Majidi R, et al. History, presence, and future of mitomycin C in glaucoma filtration surgery. *Curr Opin Ophthalmol*. 2021;32(2):148–159. doi:10.1097/icu.0000000000000729
46. Han R, Zhong H, Zhang Y, et al. MiR-146a reduces fibrosis after glaucoma filtration surgery in rats. *J Transl Med*. 2024;22(1):440. doi:10.1186/s12967-024-05170-2
47. Ameer G, Keate R, Bury M, et al. Cell-free biodegradable electroactive scaffold for urinary bladder regeneration. *Res Sq*. 2024:rs–3. doi:10.21203/rs.3.rs-3817836/v1